

Wavelength-agnostic Metasurface Design for Next Generation 2D Photodetectors

Ayush Mukund Jamdar¹, Rituraj^{2*}, Srinivas Krishnamurthy^{3,4}, Vidya Praveen Bhallamudi³, Sivarama Krishnan^{3**}

¹Department of Electrical Engineering, Indian Institute of Technology Madras, India

²Department of Electrical Engineering, Indian Institute of Technology Kanpur, India

³Department of Physics, Indian Institute of Technology, Madras, India

⁴Sivananthan Laboratories, Bolingbrook, IL 60440, USA

*Corresponding author(s)—**srkrishnan@iitm.ac.in, *rituraj@iitk.ac.in

Abstract

We explore a versatile technique for inverse design of 2D photonic crystal-based dielectric metasurfaces. These surfaces, known for their ability to manipulate light-matter interactions, can be precisely controlled to achieve specific functionalities. The key to this lies in efficiently optimizing the geometric patterns and dimensions of the metasurface. Through a composite method which exploits two well-established paradigms - Covariance Matrix Adaptation optimization and Rigorous Coupled Wave Analysis (RCWA) working together in tandem, we demonstrate our ability to design and optimize resonances in meta-elements (unit cell) to achieve desired optical performance such as near-perfect absorption at chosen wavelengths or spectral bands, which otherwise proves to be challenging or even impossible with conventional inverse design implementations. Applying this method, we realize simple and elegant structures involving just a few layers – a monolayer absorber, a transparent meta-substrate, and a rear-end reflector to achieve nearly perfect absorption, ~100%, simultaneously at one or more predetermined wavelengths. A quick convergence of our method to near-perfect absorption at 1550 nm using a layer of black phosphorus combined with a silicon metasurface proves this point. This versatile technique can be applied to tailor reflectance and transmittance for any optical mode and wavelength while keeping the metastructure design uncomplicated and easy to realize through conventional nanofabrication techniques. Consequently, this computationally efficient approach paves the way for designing high-performance 2D metasurface-based devices using well-known materials, and without the need for extensive painstaking materials engineering, for a wide gamut of applications which otherwise and hitherto known to suffer from poor, often less than desirable parameters of operation particularly in use cases such as photodetectors in the IR, high-efficiency single-photon detection in room-temperature devices as well as biphoton sources, to name a few. Thus, the impact this will have on critical components in contemporary photonic quantum technologies, integrated photonic circuits for optical communication as well as in nonlinear optical realisations is imminent and foreseeable.

Introduction

In their seminal study (1), Piper *et al.* demonstrated that a photonic crystal structure (PCS) can significantly enhance the absorption of 1550 nm light in a graphene monolayer from a mere 2.3% (2) to a total absorption of 100% by inducing resonance. This is in stark contrast to the traditional

photodetectors which often require a few-micron-thick absorber for efficient light absorption. However, this comes with the caveat that a thicker absorber leads to increased dark current lowering device sensitivity. By enabling efficient absorption in ultra-thin layers with PCS can lead to photodetectors with inherently ultra-low dark current as well as higher operating temperatures (3) - (5).

A key insight from this approach to device design (1) is that the optical performance depends solely on the geometric parameters of the metastructure, both the parameters that govern its long-range ordering, its periodicity, as well as those that define its unit cell - thickness, and pattern type - for fixed material composition. The dependence on material properties and their limitations are overcome and transcended by this powerful tool for designing resonances at any desired wavelengths to tailor optical responses beyond that achievable by conventional approaches, hitherto. This strategy towards device design impacts the development of photonic devices for a wide range of applications with very unique needs.

Total absorption of narrowband around a single wavelength is required in sensing and optical communications (6). Ostensibly, in dual-wavelength scenarios such as non-degenerate time-resolved pump-probe type measurements (7), nonlinear harmonic conversion devices such as second harmonic generation (SHG) requiring intense primary input light beams which are often converted to relatively weak harmonic outputs at desired wavelengths (8), or essential quantum optic photon sources, bi- or entangled-photon, sources which rely on energy-momentum conserving nonlinear optical parametric down conversion where a pump photon following its interaction with material is converted to a pair of useful daughter photons at wavelengths different from the parent pump, double resonant designs are much needed, yet, rare to find. In optical communication systems, simple designs for seamless channel switching and efficient operation at both $1.3\text{ }\mu\text{m}$ and $1.55\text{ }\mu\text{m}$ wavelengths are much needed (9), as are add-drop optical filters that selectively transmit specific wavelengths while rejecting others (10). Furthermore, tunable implementations of such devices exploiting unique material properties, such as those offered by phase change materials, PCMs, to retain the high-optical performance of metastructure designs are well-poised to disrupt hyper-spectral imaging (11). Thus, the ability to design resonances through metasurfaces is crucial to meet both the unique and diverse requirements these evidently important applications place on tailoring device responses, leading to enhancements in their performance, often beyond the limits of primitive designs and architectures.

From a practitioner's perspective, methods to design these metasurfaces can be classified into *forward* and *inverse* design. Traditionally, forward design either utilizes an exhaustive search through the metasurface parameter space or a priori intuitive knowledge. However, when complex designs with more dimensions (degrees of freedom) are required to attain highly constrained optical modes, complete exploration of the design space becomes computationally implausible and unrealistic. Moreover, intuitive methods cannot guarantee a globally optimal solution. On the other hand, inverse design methods include topology optimization, machine learning techniques, and evolutionary algorithms (12). As discussed in (12), topology optimization uses gradient-based local optimizers that are not guaranteed to find the globally best solution since the metasurface parameter space typically involves several local optima. In machine learning techniques, a large dataset must be generated using electromagnetic simulations. The required training data for a problem scales up exponentially as device complexity increases through dimensions (13).

Interestingly, evolutionary algorithms provide a reliable solution to inverse design through stochastic numerical optimization. Methods like genetic algorithms (14), Ant-Colony Optimization (ACO) (15), and Particle Swarm Optimization (PSO) (16) have been applied to metasurface design. In particular, the Covariance Matrix Adaptation – Evolutionary Strategy (CMA-ES), based on adaptive sampling, provides

faster convergence and more accurate results (17). An application of CMA-ES to 3D GaN phase gradient metasurfaces made of nanopillars of different shapes, targeting maximum light deflection efficiency, is demonstrated in Elsawy *et al.* (17). However, for PCS-based applications discussed earlier, a general design method needs to be developed. In this article, we develop such a method by combining CMA-ES and Rigorous Coupled Wave Analysis (RCWA) (18) – a highly efficient Maxwell's equation solver for layered structures invariant along the z direction. The proposed approach significantly improves the efficiency of photodetector design by eliminating the need for exhaustive searches in high-dimensional parameter spaces. The successful development of such a tool holds significant promise for various applications in photonics, communication, and sensing, where tailored light absorbers are in high demand. In what follows, we enunciate our method, approach, and results.

An Inverse Design Approach

Our approach is to systematically optimize the PCS design for controlling the parameters absorbance, reflectance, and transmittance in the desired optical modes, either all of them simultaneously or otherwise. This method is agnostic to the choice of materials and the targeted optical modes characterized by wavelength, polarization, and angle of incidence. Although the methodology and strategy can be easily adapted to any of the optical parameters and properties of the systems, i.e., tailoring absorbance, reflectance, and transmittance, we limit this discussion to designing photodetectors with increased absorbance.

To demonstrate our algorithm, we implement a three-layered photodetector design made of 7-layered (4 nm) black Phosphorus (bP) (19) as a 2D material for light absorption, non-absorbing silicon (with real and imaginary parts of the refractive index $n=3.5$ and $k=0$, respectively) as the material for the photonic crystal substrate, and a metallic mirror reflector at the bottom, as shown in Figure 1.

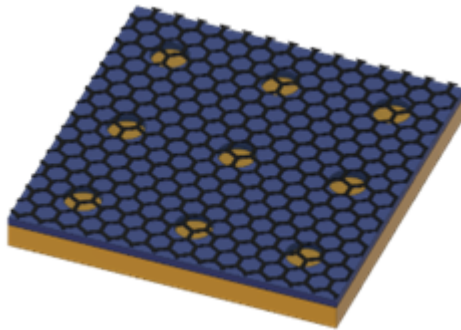


Figure 1: This schematic represents the three-layered structure used to design photodetectors. The top mesh represents the 4 nm thick 7-layered black phosphorus, the blue layer with holes is the patterned Silicon metasurface, and the bottom yellow layer represents a lossless metallic mirror.

Given the following information:

- a) refractive indices of all materials denoted by Θ ,
- b) a set of geometrical shapes and patterns, and
- c) a set of target wavelengths and optical modes $\Lambda = \lambda_1, \lambda_2, \dots, \lambda_N$,

we need to design a metasurface that supports resonances, leading to high absorption at these wavelengths. In this case, we use a cylindrical hole with a circular cross-section in Si, i.e., a 2D periodic square array of unfilled air holes in Si, for designing the PCS. However, the same method can also be applied to any other cross-sectional pattern, like polygonal holes or apertures. We chose the circular

cross-section with smooth edges since these are realistic to fabricate as against those with sharp corners/edges. Thus, the optimizable geometric parameters, as shown in Fig. 2, are periodicity l of the square lattice, thickness t of the PCS, the position of the centre of the hole in the unit cell $c = (c_x, c_y)$, and the radius of the corresponding hole r . Further in this study, we allow for the possibility of a number of hole centres $N_0 > 1$ in the unit cell, even allowing partial hole as in Fig. 2.

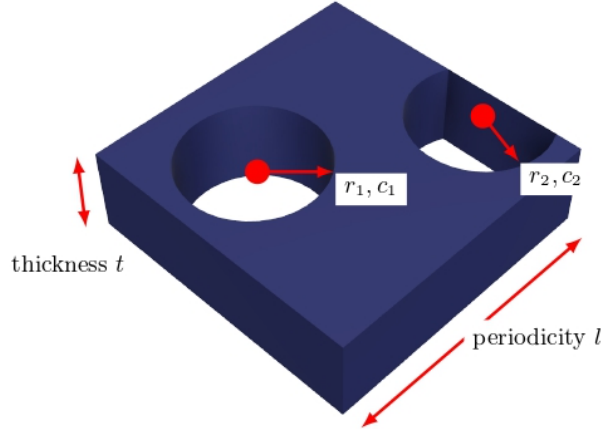


Figure 2: A schematic showing the metasurface unit cell and its optimizable geometric parameters – thickness t , periodicity l , hole radii (r_1, r_2), and hole centers (c_1, c_2) – a case with more than one hole. In this case, the second hole partially occupies the unit cell. Upon building a lattice of these unit cells, the desired PCS is created.

For optimization over multiple target wavelengths or optical modes, i.e., cases where $N > 2$, we allow for $N_0 > 1$ holes per unit cell to have more degrees of freedom and, thus, a higher dimensional search space to find the optimal structure. These holes may or may not be allowed to intersect. Therefore, in general, we will have $3N_0 + 2$ optimization variables- the position of the center within a unit cell and the radius, of each hole, as well as the periodicity and thickness of the PCS, each of which is bounded to remain within a range of feasible values, signifying box constraints, Ω_i for $i = 1, 2, \dots, 3N_0 + 2$. By specifying such a feasible set for each dimension, we can control and limit the search space. Let X denote the vector of geometry variables. We have $X \in \Omega \subset \mathbb{R}^{3N_0+2}$. As mentioned, absorption would be a function of these geometric parameters and the material refractive indices. Formalizing this mathematically, we define the absorption function for the photonic crystal $A: (\lambda, \Omega, \Theta) \rightarrow [0, 1]$ for wavelength $\lambda \in \Lambda$. To find the best conditions for employing this PCS as the active component of a photodetector, we wish to find the optimal metasurface geometry X^* such that,

$$X^* = \arg \max_{X \in \Omega} \sum_{i=1}^N A(\lambda_i, X, \Theta) \quad (1)$$

Electromagnetic calculations

To calculate the optical response of our metasurface designs, we employ rigorous coupled wave analysis (RCWA) (18). This technique solves Maxwell's equation in the frequency domain by spatial discretization in the direction normal to the layer, whereas, within each layer, they are solved analytically in the Fourier domain. RCWA is a well-established method for analysing layered periodic structures, favoured for its high computational efficiency and speed. In this work, we performed all simulations using a Python implementation of RCWA known as GRWCA, cf. ref. (20). Additionally, we leverage Poynting vectors calculated at layer boundaries to determine the layer-wise absorption profile within the metasurface.

Optimization

The absorption function A , as defined above, is a complex, non-convex, non-separable, and rugged (multiple local optima) function, the direct gradient of which is not explicitly computable. Thus, we require a stochastic numerical optimization technique. As discussed in (17), to find global maxima in this case, the CMA-ES stochastic optimization algorithm proves to be a particularly well-suited tool due to the nature of the absorption function. For a detailed explanation of the algorithm, we refer the reader to references (21), (22), and (23).

Essentially, the CMA-ES algorithm treats all the design parameters as random variables drawn from a multivariate Gaussian distribution. The core concept herein lies in iteratively evolving the mean and covariance matrix of this distribution to guide the search towards promising regions of the design space. During each iteration, CMA-ES updates the mean of the distribution to favour previously successful candidate solutions, i.e., those with better objective function values. Simultaneously, the covariance matrix is also adaptively updated to favour search directions that have led to past improvements. This algorithm explained in Figure 3, requires an initial mean vector m_0 constituting initial values for all the parameters in the metasurface geometry X . Each metasurface parameter is subject to a bound constraint specified by Ω_i introduced earlier, defining a continuous range of allowed values. We initialize the unit cell dimensions, namely, its period and thickness, within this search space and the hole radii with random values. Notably, in the case of a single hole ($N_0 = 1$), the hole center is initially positioned at the center of the unit cell, corresponding to complete holes within each unit cell, which is the preferred solution. However, the optimization process can shift the hole center, potentially leading to partial holes, see Fig. 2 depending on the specific problem and the optimal design. Altogether, this creates the mean vector m_0 , an initial guess composed of initial values for all design parameters.

In addition to m_0 , the algorithm requires a hyperparameter σ_0 – the initial step-size. The CMA-ES algorithm dynamically adapts the step-size using cumulative step-size adaptation (CSA). This step-size controls the search "reach" in each iteration, balancing the exploration of new regions in the initial stages with focused exploitation around promising areas as the search progresses. σ_0 and m_0 should be such that the optimum presumably lies within the initial high-dimensional cube $m_0 + 3\sigma_0(1, \dots, 1)^T$. It is suggested that given a search space $\Omega_i = [a, b]$, one may start with $\sigma_0 = 0.3(b - a)$ (21). In our experiments, we typically used $0.5 < \sigma_0 < 1.0$. Overall, the hyperparameters and initializations required by the algorithm are m_0 , σ_0 , Ω_i for each variable, and the number of holes per unit cell N_0 . However, an informative guess for m_0 would often lead to the best results faster than a random m_0 , i.e., the convergence time depends on this starting point. For instance, if the initial hole radius is too small or too large for a small unit cell, finding the solution may be difficult as the PCS might not play its role. Due to the stochastic nature of CMA-ES and the random start, multiple optimization trials, typically 5-10, might be necessary to achieve the best design. Here, we note that due to the nature of the algorithm's code implementation in Python, the objective function is minimized by default. Hence, we minimize the sum of reflectivity and transmissivity to maximize absorptivity for a layer.

The algorithm stops on a few termination criteria related to numerical stability described in (21). The ones most relevant for this application are stagnation and function tolerance. The stagnation criterion checks if the designs have not improved over several generations by comparing the median of the last few values with the first. For a minimization problem, the tolerance criterion halts the process if the function value falls below a threshold, typically 10^{-10} . Exploiting the scale invariance of Maxwell's equations, we normalize all lengths used within the optimization process to a base unit length of 1

micron. This allows us to treat them as dimensionless quantities that can be processed for numerical optimization. In the following section, we further describe present representative results that demonstrate power and application of this method.

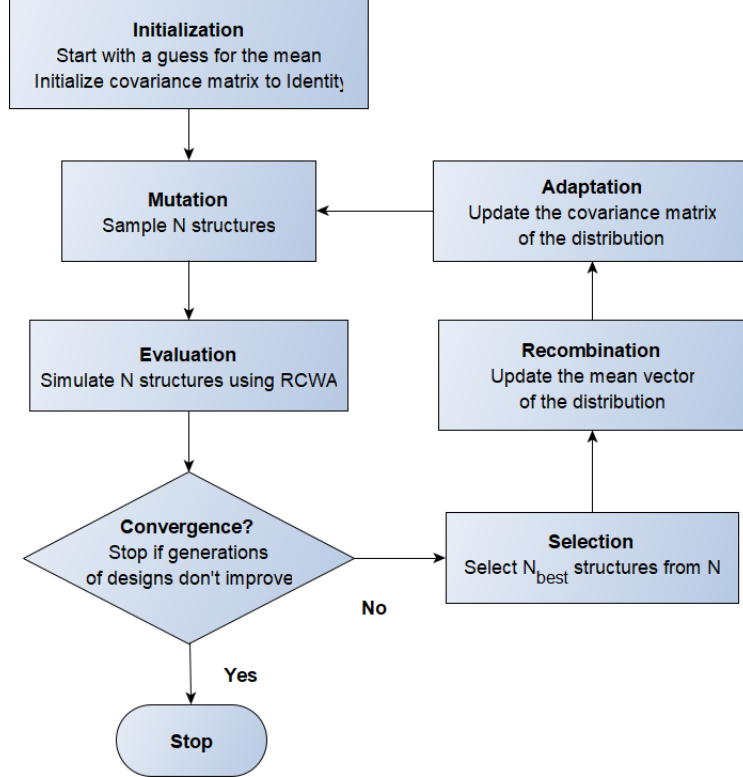


Figure 3: The CMA-ES Algorithm for photodetector design as explained in (17). We start with an initial guess for the mean of all design variables. From a few samples drawn from the Gaussian and simulated through RCWA, the best few are selected to update the mean and covariance. The distribution keeps updating until no significant improvement is observed in sampled designs.

Results and Discussion

The following simulations were performed on a single core of the Dual Intel Xeon Gold 6248, 20-core 2.5 GHz CPU Node at the High-Performance Computing Facility, IIT Madras. Typically, the optimization runs may require from a few minutes to two hours of runtime, depending on the problem's complexity.

Single resonance at 1.55 μm

Efficient light absorption at specific wavelengths in the infrared range is crucial for various applications in telecommunications and optoelectronics. The wavelengths of 1.55 μm and 2.1 μm hold particular importance for free space communication. Additionally, in optical communication systems, 1.55 μm coincides with the minimum attenuation window in silica fibers, making it the dominant wavelength for long-distance data transmission (24). Efficient absorbers at 1.55 μm are essential for developing critical components like sensors, optical modulators, and terminators within these systems. Photodetectors operating at an atmospheric transmission wavelength of 2.1 μm are crucial for applications such as imaging (25), sensing (26), and high-speed communication (27).

The bP exhibits a highly tuneable bandgap, ranging from 0.3 to 2 eV (28). This tunability allows for the choice of the material for the bandgap required chosen wavelength. bP is chosen to be an active absorber for infrared photodetectors considered here. In our studies, we use seven layers (4 nm thick) of bP and the measured extinction coefficient (19). We assume a normally incident plane wave on the absorber and optimize the absorption at the target wavelengths.

Our design for high absorption in 1.55 μm , schematically shown in Fig. 1, consists of bP on Si PCS with a metallic reflector. We used a 2D periodic array of one hole per unit cell ($N_0 = 1$) and optimized the parameters periodicity, thickness, hole radius, and hole center for the highest absorption. Figure 4(a) shows nine-unit cells of the optimized metasurface design obtained from CMA-ES in 8 minutes of runtime. The absorption in bP, calculated by integrating the Poynting vector in bP, is plotted (blue) as a function of wavelength (Fig. 4(b)). We see that 100% absorption at 1.55 μm and over 80% absorption within ± 30 nm from the central wavelength. When the optimized design parameters are rounded off to the nearest 5 nm, the calculated absorption (orange) changes only very little, indicating that the design is robust to fabrication variations.

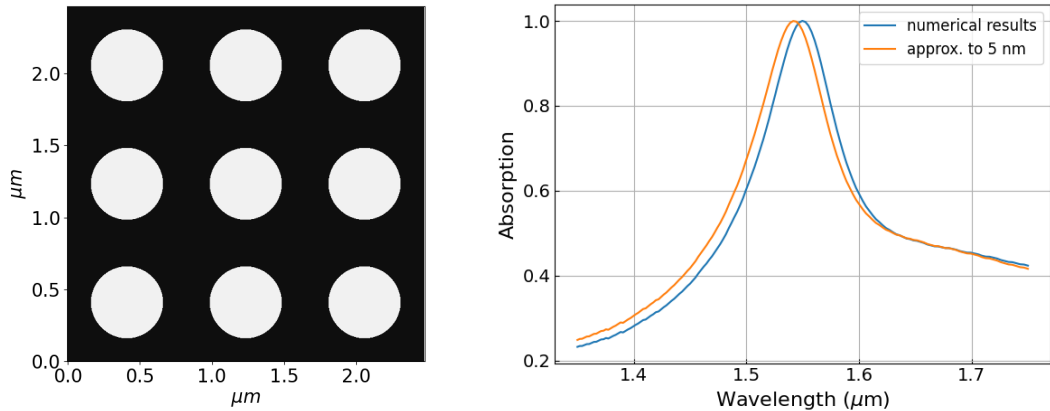


Figure 4: (a) The periodic array ($r = 253$ nm, $l = 823$ nm) of holes in silicon ($t = 131$ nm) for a photodetector operating at 1550 nm. (b) Absorption (blue) in bP. The algorithm provides real numbers of arbitrary precision for each design variable. We rounded off the values for r , l , and t to the nearest 5 nm and calculated the absorption (orange).

Single resonance at 2.1 μm

To design a photodetector for 2.1 μm , we replaced the metallic reflector with a distributed Bragg Reflector (DBR) mirror made of alternating SiO_2 and Sb_2S_3 layers (Figure 5). Since a DBR is not reflective to all wavelengths, this design is aimed to test if the algorithm remained effective even without a perfect and broadband reflector. In this case too, the metasurface design variables X remain the same as before. Figure 6(a) shows the optimized metasurface design generated in just 20 minutes of runtime. The calculated absorption in bP is plotted in Fig. 6(b). We see that absorption at the designed wavelength of 2.1 μm is 100% but with a narrower (± 10 nm) band of absorption of over 80%. Additionally, we see unintended resonances at a few nearby wavelengths. Clearly, it is advantageous to have a broadband reflecting ground place. Nevertheless, perfect absorption with an ML of material can be achieved leading photodetector with negligible dark current and near-perfect photocurrent.

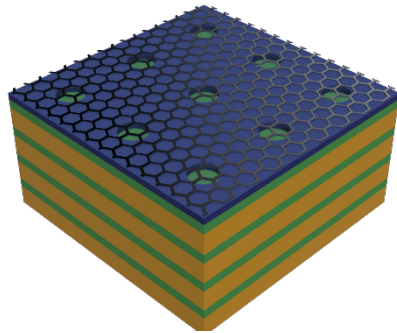


Figure 5: Schematic of the system used to design a photodetector for 2.1 μm . The top mesh represents Black Phosphorus; the blue layer with holes is the patterned silicon metasurface. The metal layer from the previous design (Fig. 1) is replaced with a DBR mirror of alternating SiO_2 (green) and Sb_2S_3 (orange) layers.

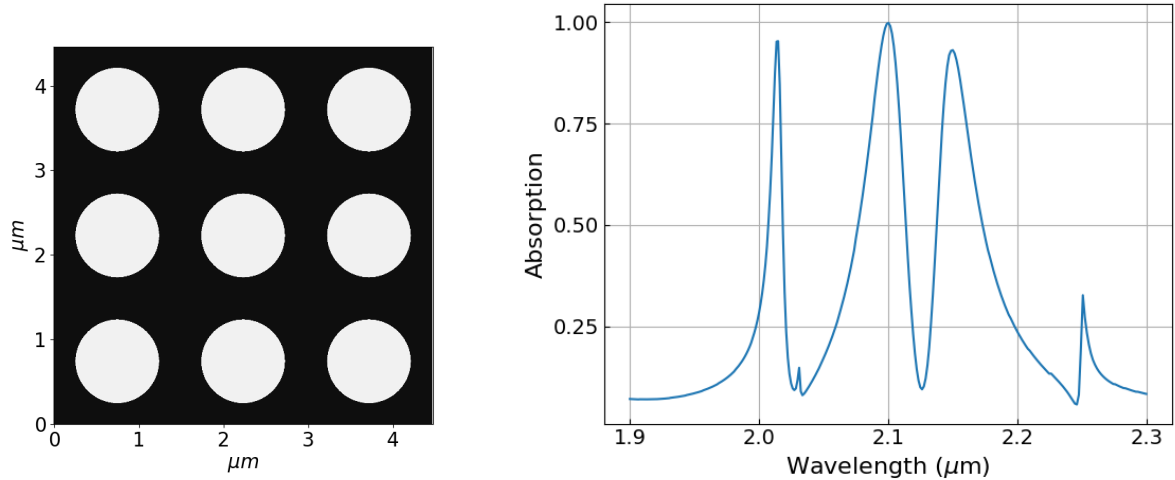


Figure 6: (a) The periodic array ($r= 499 \text{ nm}$, $l= 1.48 \mu\text{m}$) of holes in silicon ($t=113 \text{ nm}$) for a photodetector operating at 2.1 μm . (b) Absorption in bP.

Resonance at Two Wavelengths

Next, we apply our method to design a PCS that supports double (or multiple) resonances at the chosen wavelengths 1.3 μm and 1.55 μm . This design is highly desirable for seamless channel switching and simplified system design in optical communications (9). Using the same three-layered structure (bP, silicon, metal as in Fig. 1), we employed the CMA-ES technique to design double resonance. We kept $N_0 = 1$ to enable faster search in a small search space. The nine unit cells of the metasurface obtained through 53 minutes of optimization runtime are shown in Figure 7(a). Note that the unit cell does not contain one full hole. This creates a bit complicated structure for fabrication as a trade-off for a larger search space to solve a more demanding optimization problem. The absorption spectrum of this optimized structure is plotted in Figure 7(b), which shows resonant absorption peaks in bP at both wavelengths of interest. The absorption is nearly 100% at 1.55 mm but is only $\sim 80\%$ at 1.33 mm. A larger search space (more complicated design) is required to get near-perfect absorption at both wavelengths.

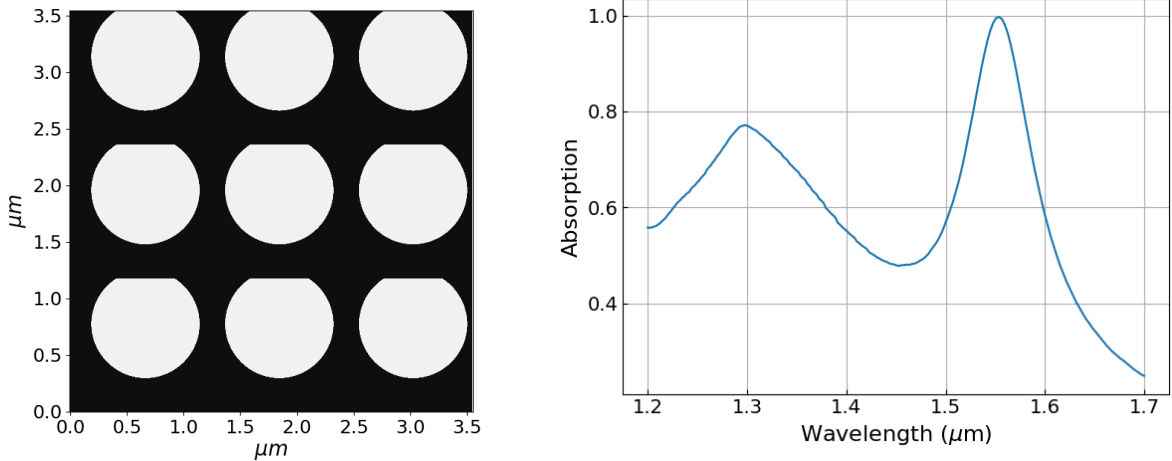


Figure 7: (a) The silicon PCS design ($r = 482$ nm, $l = 1.18$ μm , and $t = 109$ nm) for high absorption at 1.3 and 1.55 μm . As the number of target absorption wavelengths increases, more degrees of freedom are required. We allow the hole to partially leave the unit cell to enable that, thus creating an asymmetric structure with partial holes. (b) Absorption in bP.

Wide-Incident Angle Absorption

So far, we have optimized the metasurface for normal incident plane waves. However, often the detectors will be realistically required to have high absorption for an optical mode finite spot size comprised of plane waves with wave-vectors lying in a cone of incidence. Here, we show that the same inverse design optimization procedure can be used not only to design and improve a spectral response but also an angular response. Such a design for 1.55 μm is illustrated in Figure 8. Using the three-layered structure as before, we designed a metasurface that will enable wide-incident angle absorption in bP (Fig. 8b). To do so, we uniformly sampled a few points in the range $[0, \theta_{\max}]$ and try to maximize absorption at each of these discrete angle samples. One may use any type of incident light polarization – TE or TM, or a combination of both, in RCWA. However, in this example, we use s-polarized (TE) light. We observe that the designed structure exhibits at least 80% absorption in a 30-degree cone of incidence, whereas the FWHM exceeds 40° . This optimization was performed in 90 minutes of runtime.

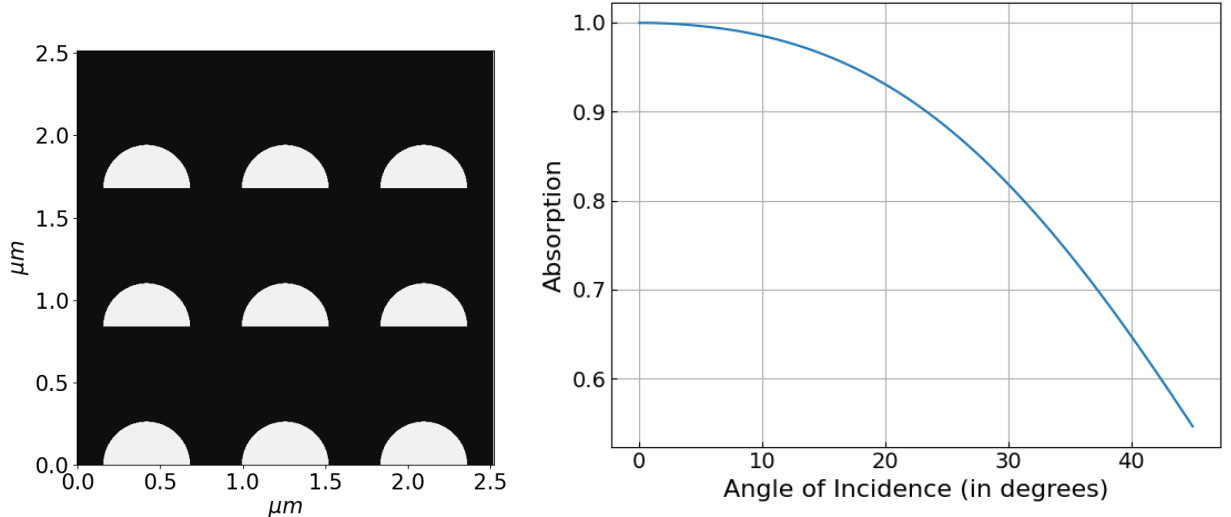


Figure 8: (a) The periodic array ($r = 266$ nm, $l = 838$ nm) of almost semi-circular holes in silicon ($t = 126$ nm) for a photodetector absorbing a wide-incident angle cone of s-polarized light at $1.55 \mu\text{m}$. (b) Absorption in bP.

Discussion:

As seen in the optimization for double resonant wavelengths and wide-angle absorption, we traded off hole symmetry and introduced complexities in the design to meet more stringent requirements. When more resonances are desired, more complicated structures may be required. Furthermore, one may tune hyperparameters like N_0 to have two or more such holes per unit cell. One could also work with a triangular lattice of holes. However, like any practical optimization problem, there will be a practical limit to the number of different resonances that can be designed. This heavily depends on the choice of materials and pattern type from a physics perspective. Nevertheless, limitations can be tackled by experimenting with hyperparameters, patterns, and the objective function used to frame the optimization problem.

Multiple avenues exist to improve this inverse design procedure through mathematics and physics. One can experiment with various metasurface layers by optimizing them together or sequentially. Furthermore, a staircase approximation is required to simulate conical holes or curved cavities as RCWA only deals with layers invariant along the z-axis. However, this can quickly become expensive. Mathematically, in equation (1), we can explore possibilities by changing the summation to a weighted sum or a product of individual objective functions. Interestingly, it might also be possible to draw inferences from the photonic band diagrams of such structures to gain deeper insights into how the shape of the cavity influences optical response. This analysis might be instrumental when an excellent initial guess is required; the algorithm can further improve upon that.

Conclusion

In conclusion, we have developed a powerful technique for inverse designing periodic dielectric metasurfaces by efficiently optimizing the geometric patterns and dimensions of the metasurface. As a demonstration of the method, we applied it to design metasurface structures to achieve near 100% absorption at the chosen wavelengths of $1.55 \mu\text{m}$ and $2.1 \mu\text{m}$ with a monolayer of 2D material. The ability to achieve near perfect absorption at single wavelength will be useful in designing single photon avalanche photo detectors operating at room temperature. In addition, this method is applied to

achieve double resonances in an integrated cavity structure to demonstrate its possible use in efficient pump-probe, second harmonic conversion, and biphoton production experiments.

Acknowledgements

We acknowledge the use of the computing resources at HPCE, IIT Madras. S. K. acknowledges support through the Indo-French Center for Promotion of Academic Research (CEFIPRA), the DST-DAAD bilateral research program of the Ministry of Science and Technology, Govt. of India, with Deutsche Akademischer Austauschdienst, and the Max Planck Society, Germany, Scheme for Promotion of Academic Research (SPARC), Min. of Education, India as well as the Quantum Center of Excellence for Diamond and Emergent Materials (QuCenDiEM) group as part of the Institute of Eminence (IoE) program (project SB20210813PHMHRD002720) at IIT Madras. Rituraj acknowledges support from Science & Engineering Research Board through project number SERB/EE/2022423.

References

1. *Total absorption in a graphene monolayer in the optical regime by critical coupling with a photonic crystal guided resonance.* **Piper, J. R., & Fan, S.** 2014, *Acs Photonics*, Vol. 1(4), pp. 347-353.
2. *A graphene-based broadband optical modulator.* **Liu, M., Yin, X., Ulin-Avila, E. et al.** 2011, *Nature*, Vol. 474(7349), pp. 64-67.
3. *Influence of photonic crystals on the performance parameters of GeSn vertical-structure photodiodes.* **Chong Li, Xinyuan Gao, Kai Guan, Weize Li, Ziyi Ma, Gang Xu, Zhanjie Li, Shuai Yang, Nan Wang, Chunlai Xue.** 2023, *Optics & Laser Technology*, Vol. 163, p. 109375.
4. *Mid-infrared integrated photonics on silicon: a perspective.* **Lin, H., Luo, Z., Gu, T., Kimerling, L. C., Wada, K., Agarwal, A., & Hu, J.** 2017, *Nanophotonics*, Vol. 7(2), pp. 393-420.
5. *Recent advances in the functional 2D photonic and optoelectronic devices.* **Wang, X., Cui, Y., Li, T., Lei, M., Li, J., & Wei, Z.** 2019, *Advanced Optical Materials*, Vol. 7(3), p. 1801274.
6. *Silicon/2D-material photodetectors: from near-infrared to mid-infrared.* **Liu, C. Y. et al.** 2021, *Light.: Science & Applications*, Vol. 10(1), p. 123.
7. *Time-resolved pump-probe experiments at the LCLS.* **James M. Glownia, J. Cryan, J. Andreasson, A. Belkacem, N. Berrah, C. I. Blaga, C. Bostedt, J. Bozek, L. F. DiMauro, L. Fang, J. Frisch, O. Gessner, M. Gühr, J. Hajdu, M. P. Hertlein, M. Hoener, G. Huang, O. Kornilov, J. P. Marangos, A. M. March, B. K. Mc.** 2010, *Optics Express*, Vol. 18(17), pp. 17620-17630.
8. *Optical second harmonic generation in plasmonic nanostructures: from fundamental principles to advanced applications.* **Butet, J., Brevet, P. F., & Martin, O. J.** 2015, *ACS Nano*, Vol. 9(11), pp. 10545-10562.
9. *All-optical wavelength switching from 1.3 μm to a 1.55 μm WDM wavelength routed network: system results.* **Chidgey, P. E. Barnsley and P. J.** 1992, *IEEE Photonics Technology Letters*, Vol. 4(1), pp. 91-94.
10. *Photonic crystal based narrowband optical filter: A brief analysis.* **Madhumitha M, Selvendran S, Sivanantha Raja A, Esakki Muthu K.** 2021, *Optik*, Vol. 228, p. 166162.
11. *Optically reconfigurable metasurfaces and photonic devices based on phase change materials.* **Wang, Q., Rogers, E., Gholipour, B. et al.** 2016, *Nature Photon*, Vol. 10(1), pp. 60-65.

12. *Empowering Metasurfaces with Inverse Design: Principles and Applications*. **Zhaoyi Li, Raphaël Pestourie, Zin Lin, Steven G. Johnson, and Federico Capasso**. 2022, ACS Photonics, Vol. 9(7), pp. 2178-2192.

13. *Deep neural networks for the evaluation and design of photonic devices*. **Jiang, J., Chen, M. & Fan, J.A.** 2021, Nature Review Materials, Vol. 6(8), pp. 679-700.

14. *Evolutionary optimization of optical antennas*. **Feichtner, T., et al.** 2012, Physics Review Letters, Vol. 109(12), p. 127701.

15. *Optimising Efficiency and Gain of Small Meander Line RFID Antennas Using Ant Colony System*. **Lewis, A., et al.** 2009, IEEE Congress on Evolutionary Computation, pp. 1486-1492.

16. *Stochastic optimization of low-loss optical negative-index metamaterial*. **Kildishev, A. V., et al.** 2007, JOSA B, Vol. 24(10), pp. A34–A39.

17. *Global optimization of metasurface designs using statistical learning methods*. **Elsawy, M. M., Lanteri, S., Duvigneau, R., Brière, G., Mohamed, M. S., & Genevet, P.** 2019, Scientific reports, Vol. 9(1), p. 17918.

18. *Design and fabrication of blazed binary diffractive elements with sampling periods smaller than the structural cutoff*. **Lalanne, P., Astilean, S., Chavel, P., Cambril, E. & Launois, H.** 1999, JOSA A, Vol. 16(5), pp. 1143–1156.

19. *Infrared fingerprints of few-layer black phosphorus*. **Zhang, G., Huang, S., Chaves, A., Song, C., Özçelik, V. O., Low, T., & Yan, H.** 2017, Nature communications, Vol. 8(1), p. 14071.

20. *Inverse design of lightweight broadband reflector for relativistic lightsail propulsion*. **Jin, Weiliang and Li, Wei and Orenstein, Meir and Fan, Shanhui.** 2020, ACS Photonics, Vol. 7(9), pp. 2350-2355.

21. *The CMA evolution strategy: A tutorial*. **Hansen, N.** 2016, arXiv preprint, p. 1604.00772.

22. *Completely derandomized self-adaptation in evolution strategies*. **Hansen, N., & Ostermeier, A.** 2001, Evolutionary computation, Vol. 9(2), pp. 159-195.

23. *Reducing the time complexity of the derandomized evolution strategy with covariance*. **Hansen, N., Muller, S. & Koumoutsakos, P.** 2003, Evolutionary Computation, Vol. 11(1), pp. 1-18.

24. *Conquering the Rayleigh scattering limit of silica glass fiber at visible wavelengths with a hollow-core fiber approach*. **Gao, S. F., Wang, Y. Y., Ding, W., Hong, Y. F., & Wang, P.** 2020, Laser & Photonics Reviews, Vol. 14(1), p. 1900241.

25. *Si-based GeSn photodetectors toward mid-infrared imaging applications*. **Tran, H., Pham, T., Margetis, J., Zhou, Y., Dou, W., Grant, P. C., ... & Yu, S. Q.** 2019, ACS Photonics, Vol. 6(11), pp. 2807-2815.

26. *Mercury telluride quantum dot based phototransistor enabling high-sensitivity room-temperature photodetection at 2000 nm*. **Chen, M., Lu, H., Abdelazim, N. M., Zhu, Y., Wang, Z., Ren, W., ... & Zhao, N.** 2017, ACS Nano, Vol. 11(6), pp. 5614-5622.

27. *Agrawal, G. P. Fiber-optic communication systems*. s.l. : John Wiley & Sons, 2012.

28. *Layer-controlled band gap and anisotropic excitons in few-layer black phosphorus*. **Tran, V., Soklaski, R., Liang, Y. & Yang, L.** 2014, Physics Review B, Vol. 89(23), p. 235319.